tvst

Retina

High-Resolution Optical Coherence Tomography in Healthy Individuals Provides Resolution at the Cellular and Subcellular Levels

Jelena Reche[1,*], Andrea B. Stocker[1,*], Virgilia Henchoz[1], Oussama Habra[1], Pascal Escher[1], Sebastian Wolf[1], and Martin S. Zinkernagel[1]

[1] Department of Ophthalmology, Inselspital, Bern University Hospital, University of Bern, Switzerland

Correspondence: Martin S. Zinkernagel, University Hospital Bern, 3010 Bern, Switzerland. e-mail: martin.zinkernagel@insel.ch

Received: December 5, 2022
Accepted: June 7, 2023
Published: July 10, 2023

Keywords: optical coherence tomography; blue cones; photoreceptors; retinal imaging; bipolar cells

Citation: Reche J, Stocker AB, Henchoz V, Habra O, Escher P, Wolf S, Zinkernagel MS. High-resolution optical coherence tomography in healthy individuals provides resolution at the cellular and subcellular levels. Transl Vis Sci Technol. 2023;12(7):12, https://doi.org/10.1167/tvst.12.7.12

Purpose: To assess the clinical resolution capacities of a novel high-resolution optical coherence tomography (High-Res OCT).

Methods: Eight healthy volunteers were included in this observational study. Using the SPECTRALIS High-Res OCT device (Heidelberg Engineering, Heidelberg) macular b-scans were taken and compared with b-scans acquired with a SPECTRALIS HRA+OCT device (Heidelberg Engineering, Heidelberg). High-Res OCT scans were also compared with hematoxylin and eosin–stained sections from a human donor retina.

Results: High-Res OCT allowed identification of several retinal structures at the cellular and subcellular levels, namely, cell nuclei of ganglion cells, displaced amacrine cells, cone photoreceptors and retinal pigment epithelial cells compared with the commercial device. Rod photoreceptor nuclei were partially detectable. Localization of cell type–specific nuclei were confirmed by histological sections of human donor retina. Additionally, all three plexus of the retinal vasculature could be visualized.

Conclusions: SPECTRALIS High-Res OCT device provides improved resolution compared with the conventional SPECTRALIS HRA+OCT device and allows to identify structures at the cellular level, similar to histological sections.

Translational Relevance: High-Res OCT shows improved visualization of retinal structures in healthy individuals and can be used to assess individual cells within the retina.

Introduction

An understanding of the structural changes in the choroidal and retinal layers at cellular and subcellular level is important for comprehension of retinopathies such as age-related macular degeneration or retinitis pigmentosa.[1–3] The localization of cell nuclei is an important marker to monitor developmental processes and pathologic states in the retina.[4] Previous technologies are mostly invasive or performed ex vivo. Consequently, in vivo imaging of cell state and microscopic changes is an important current research topic.[5]

Optical coherence tomography (OCT) images are comparable to histological sections. To achieve cell-level imaging, axial resolution greater than 5 µm is required.[6] Noninvasive spectral domain OCT (Spectralis HRA-OCT), generating high-resolution cross-sectional images of the retina, is the gold standard in retinal diagnostics and follow-up of diseases.[7] According to the International Nomenclature for Optical Coherence Tomography INOCT 2014, the ganglion cell layer, nuclear layers, Henle's nerve fiber layer, the protein-rich (myoid) zone of photoreceptor inner segments, and outer segments of the photoreceptors show low reflectivity signals. The rest of the retinal layers appear high in reflectivity.[8] Nevertheless, there remains debate and controversy about the origin of reflectivity, especially in the outer retina.[9] To our best knowledge, it has not been possible to differentiate reflectance patterns that correspond

with cell nuclei in conventional Spectralis HRA-OCT up to now.

So far, only a few studies show visualization of cellular features by using enhanced technology such as visible light OCT or adaptive optics OCT.[10,11] However, both systems have their limitations and challenges when it comes to implementation in clinical practice.

In March 2021, a new investigational research device called the SPECTRALIS High-Res OCT, developed by Heidelberg Engineering GmbH, was introduced. With increased axial resolution of down to 3 µm and a fast image acquisition time, High-Res OCT provides more information about anatomical features whose reflection sources need to be evaluated and could yield important clinical information.[12]

The aim of our study was to determine the resolution capacities of High-Res OCT in vivo and compare these with histology. To the best of our knowledge, this study is the first to address this topic with the SPECTRALIS High-Res OCT.

Methods

Study Design

In this single-center, prospective, observational study, subjects were recruited from the Department of Ophthalmology at the University Hospital in Bern, Switzerland, in April 2022. Participants were given detailed information about the investigation by a physician and gave written informed consent to participate in the study. The study was conducted in accordance with the Swiss Human Research Act, the ICH guidelines of Good Clinical Practice, the Declaration of Helsinki and was authorized by the local ethics committee (BASEC-ID. 2021-D0038). Only participants without history of retinal disease were included.

Clinical Assessments

The improved High-Res OCT device (SPECTRALIS High-Res OCT- DMR001; Heidelberg Engineering, Heidelberg), which is a device under investigation, was used to obtain OCT images. It is a Spectral Domain OCT as the regular Spectralis HRA-OCT (Heidelberg Engineering, Heidelberg), except that the axial resolution in the tissue has been improved to reach a 3 µm instead of the 7 µm in the standard platform. In OCT, the axial resolution depends on two parameters: the central wavelength and the bandwidth of the light source.[13] To be more precise, it is proportional to the central wavelength square and inversely proportional to the bandwidth of the source. In the High-Res OCT device, the central wavelength was lowered from 880 nm to 853 nm and the bandwidth was enlarged from 50 nm to 137 nm. Owing to the larger bandwidth, the laser power on the eye was increased from 1.2 mW to 2.2 mW, which is still within safety limits. The lateral resolution remains unchanged compared with the regular Spectralis HRA-OCT and is equal to 14 µm.[14] automatic real time (ART) numbers were carefully fixed to ensure that the patient fixation skills are not impacting the sharpness of the image. To guarantee the fair comparison between devices, we used another functionality called "follow-up," which allows the transfer of position and scan parameters (number of a-scans, b-scans, and ART) between both platforms.

All eyes ($n = 16$) were scanned with the High-Res OCT. We measured the signal-to-noise ratio (SNR) of each macular b-scan within a scanned volume of a subject's eye ($n = 1$) acquired with Spectralis HRA-OCT and High-Res OCT. Therefore, we used the ImageJ plugin written by D. Sage and M. Unser at the Biomedical Image Group, EPFL, Switzerland.[15] For comparison, we transferred the same settings for eye tracking and ART from the Spectralis HRA-OCT to the High-Res OCT device. First, we compared the SNR of both devices in neutral pupil size and additionally we measured the SNR after medical dilation of the pupil.

In all of the following examinations medical dilation of the pupils was not required. In four of eight subjects (eyes $n = 8$), we first acquired images with commercial Spectralis HRA-OCT. The Spectralis HRA-OCT has a central wavelength of 880 nm, a spectral bandwidth of 50 nm, and an axial resolution of down to 7 µm. Subsequently, a follow-up scan with the High-Res OCT was performed in these four subjects on the same day and at the same macular location.

The scan protocol included a 20° × 20° OCT volume scan in high-resolution mode centered on the fovea with 49 b-scans and 25 ART frames (1024 a-scans per b-scan). With eye tracking and ART frames, average images were produced automatically, decreasing noise and improving image quality.

Each b-scan within a scanned volume of High-Res OCT and Spectralis HRA-OCT was evaluated individually by three reviewers and analyzed for differences. Reviewers included a senior clinical retinal scientist and first- and fifth-year ophthalmology residents. Scans with hyporeflective dots that might correspond with cellular components were chosen. Afterward, the selected b-scans were compared with hematoxylin and eosin–stained sections from a human donor retina to identify the structures by location. For histology, fixed eyes were dehydrated, paraffin wax-infiltrated (Logos

J, Milestone, Sorisole, Italy), embedded (DPH800 Embedding Center; Diapath, Martinengo, Italy), and cut in 5-µm sections (Leica RM2245 microtome; Leica, Heerbrugg, Switzerland). Sections passing through the optic nerve head were collected on Menzel microscope glass slides (Thermo Scientific, Waltham, MA), air dried overnight, and stained with hematoxylin and eosin (Carl Roth, Karlsruhe, Germany). Stained sections were digitalized in a fully automated PANNORAMIC 250 slide scanner (3D HISTECH, Budapest, Hungary; software version 2.2.0) and the caption was taken with CaseViewer 2.3 image analysis software (3D HISTECH).

To create the figures, the High-Res OCT and Spectralis HRA-OCT files were transferred to the Adobe Photoshop program. No image processing was performed.

Results

SNR of Images Taken by Spectralis HRA- and High-Res OCT

In a healthy woman's eye aged 32 years, each b-scan within a scanned volume of the macula was analyzed with respect to SNR. At natural pupil size, we measured a mean SNR of 1.67 ± 1.34 dB in Spectralis HRA-OCT images and 3.06 ± 1.07 dB in High-Res OCT images. After medical dilatation of the pupil, a mean SNR of 2.14 ± 1.2 dB was measured in High-Res OCT images.

General Findings by High-Res OCT as Compared With Spectralis HRA-OCT

A total of 16 healthy eyes of 8 participants (7 females and 1 male) with an average age of 29.63 years (range, 23–47 years) underwent retinal imaging with the High-Res OCT. In addition, eight eyes of four individuals were imaged with Spectralis HRA-OCT for comparison.

We observed a marked difference in image quality of cross-sectional b-scans between the two devices Spectralis HRA-OCT (Figs. 1A, 1A′) and High-Res OCT (Figs. 1B, 1B′). Supplementary Figure S1 illustrates a detailed perimacular cross-section of a b-scan acquired by the High-Res OCT showing all retinal layers for guidance. The optimized OCT technology with improved axial resolution provides additional details of the retina, which we could describe from the vitreous toward the choroid as

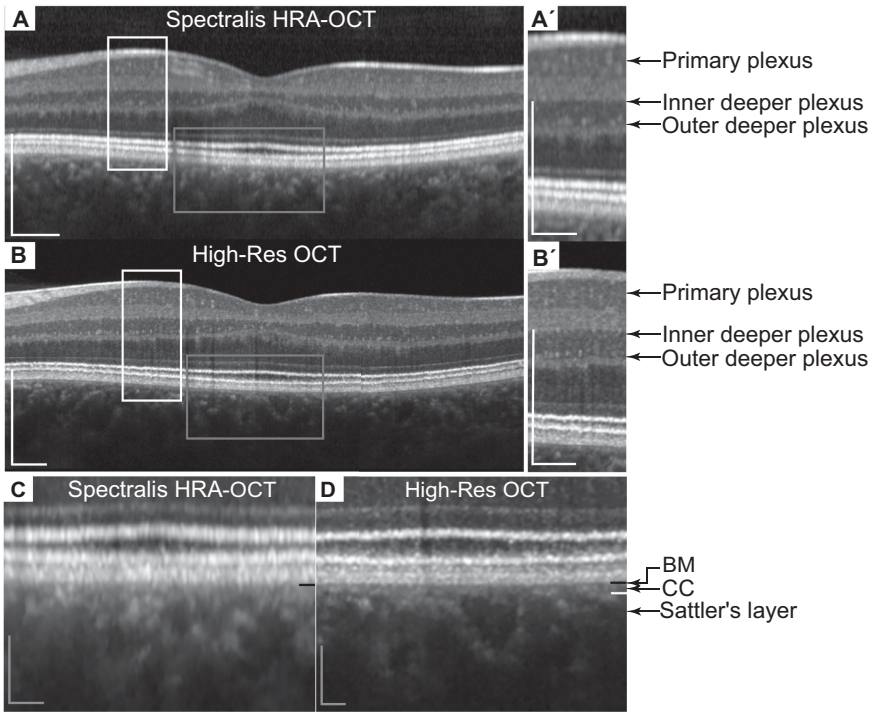

Figure 1. Comparison of OCT b-scans between Spectralis HRA- and High-Res OCT devices. Macular cross-sectional b-scan taken with spectral domain OCT (Spectralis HRA-OCT) (**A**) and High-Res OCT (**B**) and close-up view corresponding to the parafoveal white box (**A′**, **B′**) showing the retinal vascular plexus. (**C**, **D**) Close-up view of BM, choriocapillaris (CC) (inner border, *black line*; outer border, *white line*) and Sattler's layer corresponding to the grey box in the foveal area. Scale bars, white, 200 µm; gray, 50 µm.

follows (Figs. 1B, 1B′, 1D, Supplementary Fig. S1). (1) Reduced noise is best seen in the vitreous area. (2) In general, increased resolution allows for more precise delimitation of posterior hyaloid membrane and all retinal layers, especially hyper-reflective ones (internal limiting membrane, retinal nerve fiber layer, inner plexiform layer (IPL), outer plexiform layer, external limiting membrane (ELM), ellipsoid zone, interdigitation zone, retinal pigment epithelium–Bruch's membrane (RPE–BM) complex. (3) Sublayers of the IPL and RPE–BM complex can be identified. (4) Hyper-reflective vessel cross-sections of the retinal vascular plexus are more sharply imaged. (5) The choriocapillaris is demarcated more noticeably from BM (black line) and Sattler's layer (white line) (Figs. 1C, 1D). In Spectralis HRA-OCT image, only the inner border of the choriocapillaris is clearly visible (Fig. 1C, black line). (5) The retinal vasculature is observable in high detail. (6) Nuclear retinal layers (ganglion cell layer, inner nuclear layer (INL), outer nuclear layer (ONL)) show subtle variations in reflectivity that were visible with much lower contrast and clarity using Spectralis HRA-OCT. All listed features were detected in scans from all subjects.

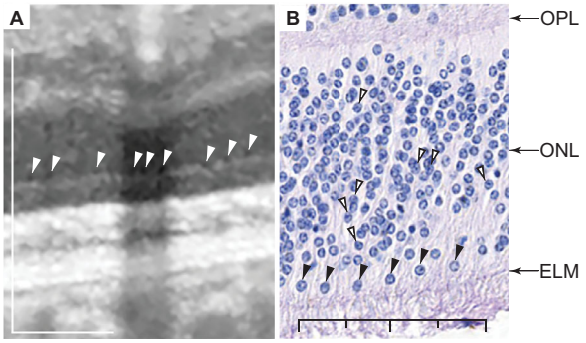

Figure 2. Cone photoreceptor nuclei identified by High-Res OCT. Both images (**A**, **B**) show an area of the outer Early Treatment Diabetic Retinopathy Study ring. (**A**) OCT b-scan captured with High-Res OCT: Hyporeflective dots (*arrowheads*) in the ONL piercing the ELM representing the cone photoreceptor nuclei. Scale bar, 200 µm. (**B**) Hematoxylin and eosin–stained histological section of a human donor retina: with basophilic nuclei of rod (*black and white arrowheads*) and cones (*black arrowheads*). Scale bar, 100 µm; original magnification ×34.1.

Identification of Retinal Cell Nuclei by High-Res OCT

We observed oval-shaped hyporeflective dots within the at the outer border (Fig. 2A, arrowheads). In some cases, the spots were even abutting the ELM. In a next step, we compared High-Res OCT images with histological specimens. In histology, cone nuclei (Fig. 2B, black arrowheads) are localized closely to the ELM owing to the shorter outer segments, when compared with rod photoreceptors (black and white arrowheads). The nuclei of the rods, in contrast, are distributed along the entire length of the ONL layer.[16] When comparing High-Res OCT images to histological sections, the oval hyporeflective spots can be found at the same location as the nuclei of cone photoreceptors in histology. Putative cone nuclei adjacent to the ELM were visible in 89.5% of High-Res OCT and in 24.2% of Spectralis HRA-OCT macular b-scans (Table 1). Thereby, the pairs of eyes show similar results.

Similarly, we were able to detect nuclei of RPE cells in High-Res OCT b-scans as hyporeflective dots at the basal site of the highly hyper-reflective RPE layer (Fig. 3A, Supplementary Fig. S2, arrows). The sizes of the five RPE nuclei highlighted with arrows in Figure 3A are listed in Table 2. We measured an

Table 1. Putative Cone Nuclei Near the ELM Are More Commonly Detectable in High-Resolution OCT Images

		Number of B-Scans of a Volume Scan Detected With Putative Cone Nuclei Adjacent to the ELM			
Subject	Eye	High-Res OCT		Spectralis HRA-OCT	
1	OD	49/49	100%	13/49	26.5%
1	OS	49/49	100%	17/49	34.7%
2	OD	57/61	93.4%	22/61	36.1%
2	OS	46/61	75.4%	19/61	31.1%
3	OD	41/49	83.7%	10/49	20.4%
3	OS	38/49	77.6%	10/49	20.4%
4	OD	44/49	89.8%	7/49	14.3%
4	OS	47/49	95.9%	5/49	10.2%
Mean		46.4/49.5	89.5%	12.9/49.5	24.2%

Right (OD) and left (OS) eyes of four subjects (eyes $n = 8$) were imaged by spectral domain OCT (Spectralis HRA-OCT) and High-Res OCT. Scanned volume consisting of 49 or 64 b-scans.

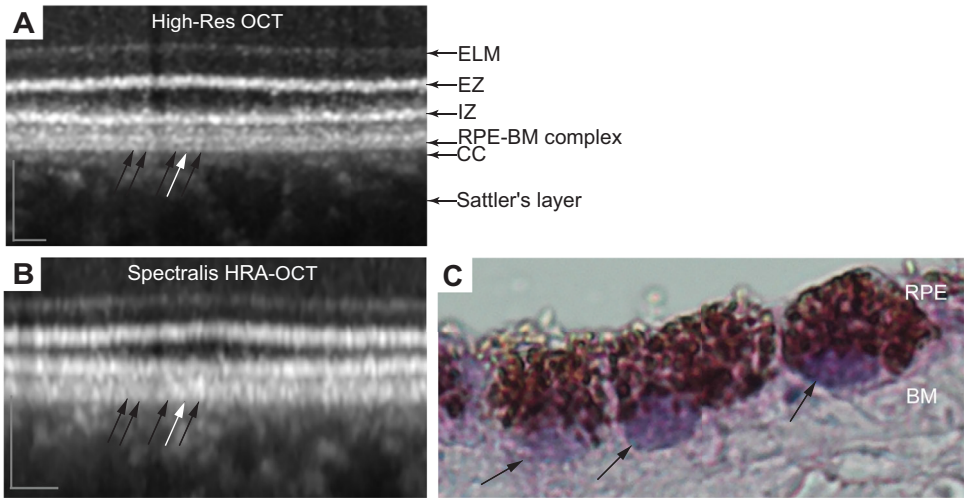

Figure 3. RPE nuclei identified by High-Res OCT. (**A**) OCT b-scan acquired with High-Res OCT showing the foveal area: Hyporeflective dots at the level of RPE correspond with RPE nuclei (*arrows*). Mononucleated RPE cell (*black arrows*), probably binucleated RPE cell (*white arrow*). The ELM, ellipsoid zone (EZ), interdigitation zone (IZ), RPE–BM complex, choriocapillaris (CC), and Sattler's layer are listed for guidance. (**B**) OCT b-scan acquired with spectral domain OCT (Spectralis HRA-OCT) representing the same area. Scale bars, 50 µm. (**C**) Hematoxylin and eosin–stained perifoveal histological section of a human donor retina with basophilic RPE nuclei (*magenta; arrows*) and underlying BM. Melanosomes and/or phagolysosomes show brown pigmentation and apical microvilli appear transparent. Original magnification ×40.

Table 2. RPE Nuclei Size in High-Resolution OCT Images

	RPE Nuclei Size	
RPE Nucleus	Vertical Diameter [Pixels]	Horizontal Diameter [Pixels]
1	5	6
2	7	6
3	6	7
4	7	10
5	6	7
Mean	6.20 ± 0.84	7.20 ± 1.64

Size of the five RPE nuclei in the foveal area marked in Figure 3A. Horizontal and vertical diameter were measured in Adobe Photoshop program [pixel].

average diameter of 6.2 ± 0.84 pixels vertical and 7.2 ± 1.64 pixels horizontal. Based on the striking larger horizontal diameter in nucleus number 4, these could be two adjacent nuclei in a binucleated RPE. These hyporeflective areas are not or barely visible on the b-scan captured with Spectralis HRA-OCT (Fig. 3B).

RPE cells in the histological section (Fig. 3C) show a typical characteristic organelle distribution. RPE cells are single layered and contain an oval magenta-stained basophilic nucleus (Fig. 3C, arrows) placed basally. Numerous pigmented granules are aggregated apically. They represent organelles such as phagolysosomes and melanosomes. The whitish to transparent structures in the apical region correspond to the microvilli of the RPE. The position of the nucleus in the histological section is consistent with the images in the High-Res OCT b-scans (Fig. 3A, Supplementary Fig. S2).

Nuclei of different cell types are identifiable within ganglion cell layer, INL, and ONL (Figs. 4A, 4 A′, 4B, 4B′). In the ganglion cell layer adjacent to the retinal nerve fiber layer, a chain of hyporeflective dots are detectable and match ganglion cell nuclei (Fig. 4A, black arrowheads). Within the IPL dispersed hyporeflective areas could represent displaced amacrine cell nuclei (Fig. 4A, black and white arrowheads). In the INL, at the border to the IPL, a row of round amacrine cell nuclei are visible (Fig. 4A, white arrowheads). The hyporeflective dots marked in the central INL are most likely bipolar cell nuclei (Fig. 4A, black arrows). In the INL next to the outer plexiform layer, a series of oval shaped hyporeflective areas most likely represent the horizontal cell nuclei (Fig. 4A, white arrows). Round hyporeflective rod nuclei can be identified in the inner ONL (Fig. 4B, arrowheads). Figures 4A′ and 4B′ are the corresponding unlabeled images.

Detailed Imaging of Retinal Vasculature by High-Res OCT

Compared with Spectralis HRA-OCT, the three retinal vascular plexus can be clearly identified by

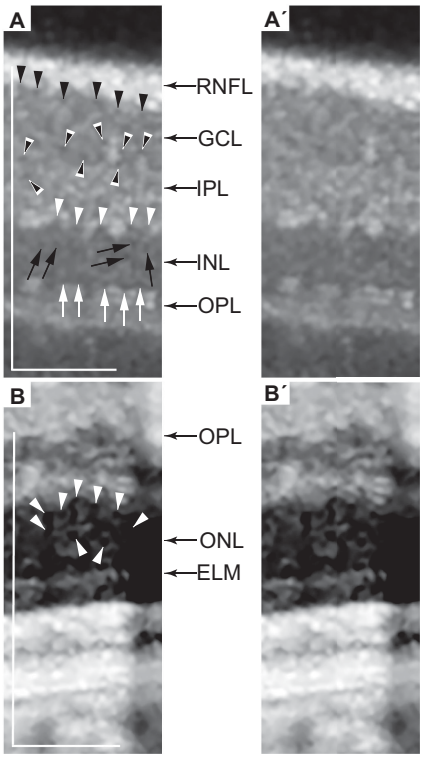

Figure 4. Cell nuclei within ganglion cell layer and ONL. OCT b-scan imaged with High-Res OCT showing a parafoveal area: (**A**) Hyporeflective roundish shaped areas interpreted as ganglion cell nuclei (*black arrowheads*) in the ganglion cell layer (GCL), displaced amacrine cell nuclei (*black and white arrowheads*) in the IPL, amacrine cell nuclei (*white arrowheads*), bipolar cell nuclei (*black arrows*) and horizontal cell nuclei (*white arrows*) in the INL. (**B**) Hyporeflective dots in the inner ONL (*arrowheads*) interpreted as rod cell nuclei. Retinal nerve fiber layer (RNLF), outer plexiform layer (OPL) and ELM are listed for guidance. Corresponding unlabeled images (A′, B′). Scale bars, 200 µm.

High-Res OCT in high detail (Figs. 1A′, 1B′, 5A, 5B). Hyper-reflective round structures represent vessel cross-sections (Fig. 5B, arrows). The primary plexus

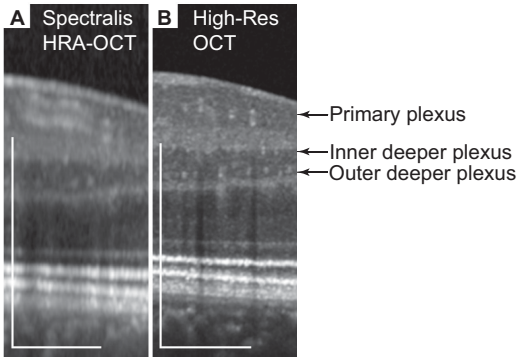

Figure 5. Retinal vascular plexus. OCT b-scan captured with spectral domain OCT (Spectralis HRA-OCT) (**A**) and High-Res OCT (**B**) showing the retinal vascular plexus in a foveal area. Scale bars, 200 µm.

can be imaged by both Spectralis HRA and High-Res OCT devices. In the Spectralis HRA-OCT b-scans, the delineation of the IPL and outer plexiform layer is challenging, so the inner and outer deeper plexus cannot be detected. Artifactual shadow projections from large blood vessels are clearly delineated by High-Res OCT when compared with Spectralis HRA-OCT images.

Discussion

This study provides the first cellular and subcellular descriptions of retinal structures in human cross-sectional macular b-scans acquired with the noninvasive SPECTRALIS High-Res OCT. A quantitative comparison of b-scans showing cone nuclei piercing the ELM was performed between the two instruments Spectralis HRA-OCT and Spectralis HRA-OCT. As a quantitative reproducibility marker, we expected that the number of b-scans showing putative cone nuclei near the ELM to be similar in all pairs of eyes. This finding was confirmed, as shown in Table 1. Compared with regular Spectralis HRA-OCT, we observed improved image quality of the anatomical features of the human retina in High-Res OCT images owing to the higher axial resolution of 3 µm and higher SNR. A clearer differentiation of retinal layers, especially hyper-reflective ones, was noted, and even sublayers were observed in the IPL and RPE–BM complex. Additionally, we were able to detect black hyporeflective dots in the nuclear layers, such as putative cone photoreceptors and RPE nuclei. These dots were observed much more frequently in b-scan images obtained with High-Res OCT than in Spectralis HRA-OCT images.

Previous studies have reported that OCT images are reminiscent of histological sections.[17–19] In a porcine retina, anatomically resembling the human one, hyporeflective zones detected with Spectralis HRA-OCT along the outer half of the ONL were correlated with cell nuclei after comparison with histological and electron microscopic images.[20] The localization of the cone photoreceptor nuclei in the outer (apical) side of the ONL is preserved in the vertebrate retina.[16] Linkers of the nucleoskeleton to the cytoskeleton complexes are responsible for this distribution.[21] Cone nuclei differ from those of rods by the peripherally distributed chromatin of the nucleus. In rod nuclei, the chromatin is aggregated.[22] Using this histochemical discrimination and known localization, we were able to identify the cone nuclei in the donor retina and matched them based on their location near the ELM, their hyporeflective and oval

appearance, and their arrangement in a row on the High-Res OCT image. Of note, we detected hyporeflective spots within the ELM, in line with microscopy studies identifying cone nuclei that pierce the ELM.[23] OCT images visualize anatomical information resulting from the backscatter of light from different layers in the retina. Cell nuclei appear hyporeflective owing to their low refractive index of $n \sim 1.4$ when compared with that of the surrounding organelles ($n \sim 1.7$).[24] In one study, a three-dimensional reflectance profile of single RPE cells was obtained. The basal hyporeflective zone of the RPE with the black spots therein was attributed to presumed cell nuclei. Similar results were obtained in other studies on photoreceptor nuclei using different combined OCT methods and histological comparisons.[10,25–27] Owing to the improved resolution and lower speckle noise of High-Res OCT, dark spots within hyporeflective bands can be discovered more frequently and clearly compared with Spectralis HRA-OCT.

In addition to the visualization of cone nuclei, nuclei of the RPE could also be identified in High-Res OCT. Interestingly, 3.0% to 5.3% of human RPE cells are binucleated and this number increases with age.[28,29] Multinucleated RPE cells have been associated with cellular stress, increased reactive oxygen species production, and decreased DNA repair.[28] A three-dimensional reconstruction of the RPE monolayer to detect the amount of multinuclear RPE cells could be, therefore, a useful marker to assess RPE-associated pathologies.[30] Further pathologies where cell nuclei localization could be a useful marker to evaluate cell vitality include retinitis pigmentosa, age-related macular degeneration, and geographic atrophy.[31,32]

Limitations of this study include the small sample size, the subjective visual detection of hyporeflective points, no detailed quantitative evaluation, and the rather young average age of the subjects. However, the findings on High-Res OCT were highly consistent, and we obtained histology to corroborate our findings.

As expected, the SNR was lower in images taken by Spectralis HRA-OCT than with High-Res OCT. In our healthy subject, mydriasis did slightly decrease the SNR. This result could be caused by an increase in chromatic aberrations owing to the wider bandwidth. Factors influencing the SNR should be investigated further in a follow-up study. In conclusion, this pilot study demonstrates examples of High-Res OCT images identifying retinal cell nuclei in multiple layers in real time in vivo with a device that can be used in clinical everyday routine. In the future, objective quantitative measurement of hyporeflective points and analysis of High-Res OCT image quality in more challenging cases, such as elderly patients with age-related macular degeneration and media opacity, would be interesting to prove the superiority of the system over Spectralis HRA-OCT.

Acknowledgments

The authors thank Sebastian Rausch and Sophie Caujolle for technical advice in image export (Heidelberg Engineering GmbH, Heidelberg, Germany) and Despina Kokona (University of Bern) for help with microscopy.

Disclosure: **J. Reche**, None; **A.B. Stocker**, None; **V. Henchoz**, None; **O. Habra**, None; **P. Escher**, Novartis Pharma Schweiz; **S. Wolf**, Allergan, Bayer, Novartis, Heidelberg Engineering, Hoya, Optos, Euretina; **M.S. Zinkernagel**, Allergan, Bayer, Novartis, Heidelberg Engineering, Roche

* JR and ABS contributed equally to this work.

References

1. Yang S, Zhou J, Li D. Functions and diseases of the retinal pigment epithelium. *Front Pharmacol*. 2021;12:727870.
2. Mulfaul K, Russell JF, Voigt AP, Stone EM, Tucker BA, Mullins RF. The essential role of the choriocapillaris in vision: novel insights from imaging and molecular biology. *Annu Rev Vis Sci*. 2022;8:33–52.
3. Wang J, Li M, Geng Z, et al. Role of 11. *Oxid Med Cell Longev*. 2022;2022:7836828.
4. Zwerger M, Ho CY, Lammerding J. Nuclear mechanics in disease. *Annu Rev Biomed Eng*. 2011;13:397–428.
5. Liu Z, Kurokawa K, Hammer DX, Miller DT. In vivo measurement of organelle motility in human retinal pigment epithelial cells. *Biomed Opt Express*. 2019;10:4142–4158.
6. Pollreisz A, Neschi M, Sloan KR, et al. Atlas of human retinal pigment epithelium organelles significant for clinical imaging. *Invest Ophthalmol Vis Sci*. 2020;61:13.
7. Aumann S, Donner S, Fischer J, Muller F. Optical coherence tomography (OCT): principle and technical realization. In: Bille JF, ed. *High Resolution Imaging in Microscopy and Ophthalmology: New Frontiers in Biomedical Optics.* Cham, Switzerland: Springer International Publishing; 2019:59–85.

8. Staurenghi G, Sadda S, Chakravarthy U, Spaide RF, International nomenclature for optical coherence tomography P. Proposed lexicon for anatomic landmarks in normal posterior segment spectral-domain optical coherence tomography: the IN*OCT consensus. *Ophthalmology*. 2014;121:1572–1578.
9. Jonnal RS, Kocaoglu OP, Zawadzki RJ, Lee SH, Werner JS, Miller DT. The cellular origins of the outer retinal bands in optical coherence tomography images. *Invest Ophthalmol Vis Sci*. 2014;55:7904–7918.
10. Chauhan P, Kho AM, FitzGerald P, Shibata B, Srinivasan VJ. Subcellular comparison of visible-light optical coherence tomography and electron microscopy in the mouse outer retina. *Invest Ophthalmol Vis Sci*. 2022;63:10.
11. Pircher M, Zawadzki RJ. Review of adaptive optics OCT (AO-OCT): principles and applications for retinal imaging [Invited]. *Biomed Opt Express*. 2017;8:2536–2562.
12. Heidelberg Engineering. HighRes-OCT user manual software version SP-X1904. Heidelberg, Germany: Heidelberg Engineering; 2021:1–162.
13. Izatt JA, Choma MA, Dhalla A-H. Theory of optical coherence tomography. In: Drexler W, Fujimoto JG, eds. *Optical Coherence Tomography: Technology and Applications*. Cham, Switzerland: Springer International Publishing; 2015:65–94.
14. Cabral D, Fradinho AC, Pereira T, et al. Macular vascular imaging and connectivity analysis using high-resolution optical coherence tomography. *Transl Vis Sci Technol*. 2022;11:2.
15. Sage D, Unser MA. Teaching image-processing programming in Java. *IEEE Signal Process Mag*. 2003;20:43–52.
16. Xue Y, Razafsky D, Hodzic D, Kefalov VJ. Mislocalization of cone nuclei impairs cone function in mice. *FASEB J*. 2020;34:10242–10249.
17. Dysli C, Enzmann V, Sznitman R, Zinkernagel MS. Quantitative analysis of mouse retinal layers using automated segmentation of spectral domain optical coherence tomography images. *Transl Vis Sci Technol*. 2015;4:9.
18. Garcia Garrido M, Beck SC, Muhlfriedel R, Julien S, Schraermeyer U, Seeliger MW. Towards a quantitative OCT image analysis. *PLoS One*. 2014;9:e100080.
19. Knott EJ, Sheets KG, Zhou Y, Gordon WC, Bazan NG. Spatial correlation of mouse photoreceptor-RPE thickness between SD-OCT and histology. *Exp Eye Res*. 2011;92:155–160.
20. Xie W, Zhao M, Tsai SH, et al. Correlation of spectral domain optical coherence tomography with histology and electron microscopy in the porcine retina. *Exp Eye Res*. 2018;177:181–190.
21. Razafsky D, Blecher N, Markov A, Stewart-Hutchinson PJ, Hodzic D. LINC complexes mediate the positioning of cone photoreceptor nuclei in mouse retina. *PLoS One*. 2012;7:e47180.
22. A.J. B. *Wolff's Anatomy of the Eye and Orbit*, 8th ed. London: Hodder Education Publishers; 1997.
23. Franz V. *Lehrbuch der vergleichenden mikroskopischen Anatomie der Wirbeltiere*. Oppel A. Charleston, SC: Nabu Press; 1913:1–417.
24. Liu Z, Kocaoglu OP, Miller DT. 3D Imaging of retinal pigment epithelial cells in the living human retina. *Invest Ophthalmol Vis Sci*. 2016;57:OCT533–543.
25. Lombardo M, Serrao S, Devaney N, Parravano M, Lombardo G. Adaptive optics technology for high-resolution retinal imaging. *Sensors (Basel)*. 2012;13:334–366.
26. Yao X, Son T, Kim TH, Le D. Interpretation of anatomic correlates of outer retinal bands in optical coherence tomography. *Exp Biol Med (Maywood)*. 2021;246:2140–2150.
27. Zawadzki RJ, Choi SS, Jones SM, Oliver SS, Werner JS. Adaptive optics-optical coherence tomography: optimizing visualization of microscopic retinal structures in three dimensions. *J Opt Soc Am A Opt Image Sci Vis*. 2007;24:1373–1383.
28. Ke Q, Gong L, Zhu X, et al. Multinucleated retinal pigment epithelial cells adapt to vision and exhibit increased DNA damage response. *Cells*. 2022;11:1552.
29. Chen M, Rajapakse D, Fraczek M, Luo C, Forrester JV, Xu H. Retinal pigment epithelial cell multinucleation in the aging eye – a mechanism to repair damage and maintain homoeostasis. *Aging Cell*. 2016;15:436–445.
30. Keeling E, Chatelet DS, Tan NYT, et al. 3D-Reconstructed retinal pigment epithelial cells provide insights into the anatomy of the outer retina. *Int J Mol Sci*. 2020;21:8408.
31. Sahel JA, Boulanger-Scemama E, Pagot C, et al. Partial recovery of visual function in a blind patient after optogenetic therapy. *Nat Med*. 2021;27:1223–1229.
32. Fabre M, Mateo L, Lamaa D, et al. Recent advances in age-related macular degeneration therapies. *Molecules*. 2022;27:5089.